Rate description of the stick-slip motion in friction force microscopy experiments

Mykhaylo Evstigneev* and Peter Reimann
Universität Bielefeld, Fakultät für Physik, 33615 Bielefeld, Germany
(Received 29 October 2004; published 26 May 2005)

During the stick-slip motion of an atomic force microscope tip contacting with a uniformly moving atomically clean surface, the force developed in the cantilever spring performs random sawtoothlike oscillations resulting from the thermally activated transitions of the tip from one surface site to the next. Using escape rate theory, the probability distribution of forces is calculated numerically to deduce the time-average lateral force as a function of pulling velocity. A transcendental equation for the average force is proposed and its approximate solution is obtained. The accuracy of this analytic approximation is demonstrated via comparison with the numerical results. The analogous force-velocity relations existing in the literature are shown to be the limiting cases of low and high cantilever spring constants of our analytic approximation.

DOI: 10.1103/PhysRevE.71.056119 PACS number(s): 05.40.−a, 07.79.Sp, 68.35.Af

I. INTRODUCTION

Miniaturization of electronic and mechanical devices has necessitated a deeper understanding of processes occurring on the atomic scale. The application of an atomic force microscope (AFM) [1] to study the friction forces acting in the nanoworld has given rise to the research direction of friction force microscopy (FFM). Because of its relevance in nanotechnological studies, as well as its theoretical interest, after a pioneering work of Mate *et al.* [2], atomic friction became the subject of an increasing number of theoretical and experimental investigations [3–19].

In a typical FFM experiment [2], the tip of an AFM cantilever is brought in contact with a uniformly moving atomically clean surface by means of a normal load F_N [see Fig. 1(a)]. The interaction between the tip and surface leads to the torsional deformation of the cantilever spring. One can determine the magnitude of this deformation by optical means and thus deduce the resulting elastic force $f(t)$, which, by Newton's third law, equals the instantaneous force of friction. As a rule, the temporal evolution of the friction force proceeds in a sawtoothlike pattern [see Fig. 1(b) showing the results of our numerical simulations; the experimentally observed force evolution is similar (see, e.g., [3])]. The central quantity of interest is the behavior of the time-averaged friction force

$$\overline{f} := \lim_{t\to\infty} \frac{1}{t} \int_0^t dt' f(t') \tag{1}$$

as a function of the pulling velocity v.

It has been experimentally established [4–10] that the average force increases approximately logarithmically with velocity. This finding was interpreted [4–10] using modeling, which relies on the assumption that thermal activation plays an important role in atomic friction. A piece of direct experimental evidence supporting this assumption is the temperature dependence of friction force reported in [5], as well as the randomness of slip events.

One of the most successful approaches to atomic friction is offered by the generalization of the one-dimensional Tomlinson model to finite temperatures. Denoting the position of the cantilever tip as z [see Fig. 1(a)], its potential energy is written as a sum of the potential of interaction with the moving surface and the elastic energy developed in the (approximately) Hookean cantilever spring of stiffness $\varkappa$:

$$U(z,t) = U_0(z + vt) + \varkappa z^2/2. \tag{2}$$

The surface potential $U_0(z)$ is a periodic function of its argument with amplitude ΔU_0, periodicity a, and minima located, without loss of generality, at na, $n=0,\pm 1,\pm 2,\ldots$. The combined potential $U(z,t)$, on the other hand, has only a finite number of minima, $z_n(t)$, due to the influence of the elastic energy [see inset in Fig. 1(a)]. The stiffness $\varkappa$ describes the cumulative effect of elastic deformation of the cantilever spring, as well as the tip apex and the substrate in the contact region [6,11,12,15]. The instantaneous time-dependent force is given by

$$f(t) = -\varkappa z(t). \tag{3}$$

Including the thermal effects, the equation of motion of the cantilever tip is written in the form [5,13–15]

$$m\ddot{z}(t) + \eta\dot{z}(t) = -U_0'(z + vt) - \varkappa z + \sqrt{2\eta kT}\xi(t), \tag{4}$$

where m is the relevant effective mass, $\xi(t)$ is an unbiased δ-correlated Gaussian noise, kT is the thermal energy, and η is the coefficient of viscosity, describing the interaction with the microscopic degrees of freedom of the thermal bath.

That no jumps over multiple lattice sites are observed experimentally during the stick-slip motion suggests that inertia typically plays a minor role in the process [3], so that the dynamics of the cantilever can be regarded as overdamped (see Ref. [15] for a theoretical justification of the overdamped limit). However, even in the limit $m\to 0$, the analysis of the Langevin equation (4) is difficult without further approximations. A particularly successful approach is possible when the dynamics of the system possesses two

*Electronic address: mykhaylo@physik.uni-bielefeld.de

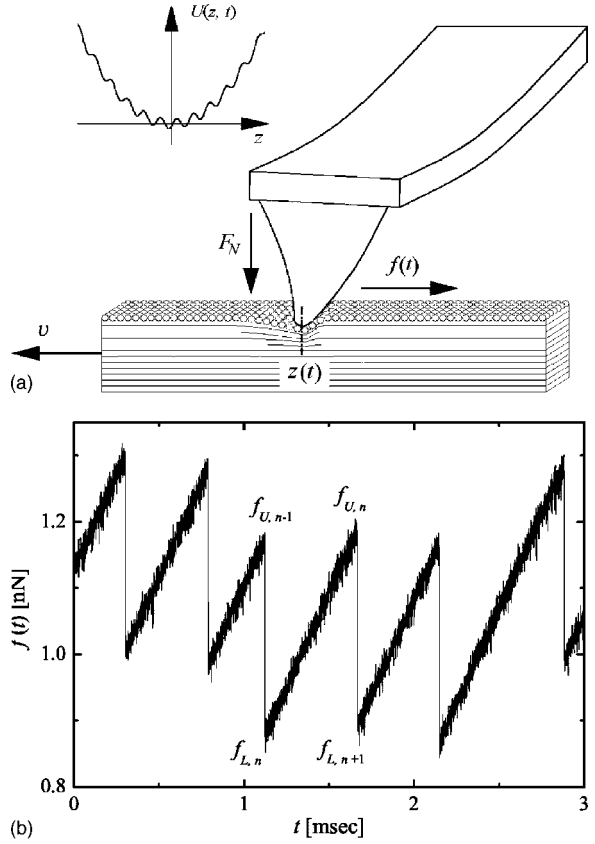

FIG. 1. (a) Schematic illustration of an FFM experiment. The inset depicts the instantaneous potential (2), in which the cantilever tip finds itself at a given instant of time t. (b) A typical example of the temporal evolution of the elastic force (3) in the stick-slip regime obtained from simulations of the Langevin equation (4) in the overdamped ($m \to 0$) limit. The lattice potential is given by Eq. (29) with parameters $\Delta U_0 = 250$ pN nm and $a = 0.52$ nm. Cantilever spring constant $\varkappa = 0.5$ N/m [8], thermal energy $kT = 4.04$ pN nm (room temperature), and the viscosity η is 1 pN msec/nm [13,15].

substantially different time scales, the shorter one characterizing the equilibration of the tip coordinate around each minimum $z_n(t)$ of the potential (2) and the longer one describing the thermally activated rare transitions between these minima. Then, it is possible to replace the dynamics of the tip coordinate $z(t)$ with that of the probabilities $p_n(t)$ to find the cantilever tip in the nth well—i.e., anywhere between the two maxima to the left and to the right of the nth minimum $z_n(t)$ of the total potential $U(z,t)$.

The qualitative picture of the resulting cantilever motion $z(t)$ under typical experimental conditions [see Fig. 1(b)] is as follows [7]. As the surface moves with respect to the cantilever base, the tip remains close to, say, the nth minimum—i.e., $z(t) \simeq z_n(t)$. The corresponding approximation for the elastic force (3) exerted by the cantilever spring,

$$f_n(t) := -\varkappa z_n(t), \tag{5}$$

constantly increases in time, leading to a reduction of the energy barrier separating the tip from the energetically more favorable adjacent minimum of the potential. Before the elastic force reaches some critical value at which this barrier disappears, the tip jumps to the lower minimum as a result of thermal activation. Then, the process repeats itself; hence, the resulting motion of the cantilever is termed the stick-slip motion.

Time-scale separation, which is a necessary condition for a rate description to apply, occurs when the relevant barrier heights are much greater than thermal energy kT [21]. This imposes certain restrictions on the system studied. In particular, it implies that the cantilever stiffness $\varkappa$ must not exceed some value, at which the potential (2) becomes monostable. This upper value can be estimated [3] as a second derivative of the surface potential at one of its minima, resulting in the condition

$$\varkappa \ll U_0''(na). \tag{6}$$

For realistic parameter values [see caption to Fig. 1(b)], this implies that the rate description is valid when $\varkappa \ll 20$ N/m. Furthermore, pulling must proceed sufficiently slowly to allow the transitions to occur before the respective time scales become comparable. Both conditions are well satisfied for most of the so-far reported experimental studies [4–8], in which the stick-slip motion is observed, whereas violation of these conditions leads to the onset of the opposite regime of steady sliding [3,16], whose consideration is beyond the scope of the present work.

Introducing the time-dependent rates $\omega_n(t) \equiv \omega(f_n(t))$ of transitions from the nth potential well to the $(n+1)$st one in the presence of the elastic force (5) and neglecting the exponentially disadvantaged transitions in the direction opposite to the elastic force, the above introduced probability of occupation of the nth potential well, $p_n(t)$, obeys the following rate equation:

$$\dot{p}_n(t) = -\omega(f_n(t))p_n(t) + \omega(f_{n-1}(t))p_{n-1}(t). \tag{7}$$

In this work, we solve the rate equation (7) in the long-time limit to deduce the probability distribution of lateral forces, which we subsequently use to estimate the time-averaged force (1) as a function of pulling velocity v. Furthermore, we deduce an approximate *analytic* relation between $\overline{f}$ and v. We demonstrate the high accuracy of this relation by comparison of its predictions with the results obtained numerically from the rate equation (7). Finally, we discuss the relation of our result to the analogous expressions existing in the literature, as well as its implications in the analysis of experimental data.

II. FORCE PROBABILITY DISTRIBUTION

As a first step, we introduce the probability $\mathcal{P}_n(t|t_L)$ of staying within the nth potential well up to the moment of time t, provided that we know with certainty that the tip was in this well at the initial time t_L—i.e., $\mathcal{P}_n(t_L|t_L) = 1$; this means that no transitions from the $(n-1)$st well to the nth one occur at $t > t_L$. The time evolution of $\mathcal{P}_n(t|t_L)$ for $t \geqslant t_L$ is governed by the rate equation of the form (7), but without the second term on the right-hand side. The solution of this equation is

$$\mathcal{P}_n(t|t_L) = \exp\left(- \int_{t_L}^{t} dt' \, \omega(f_n(t')) \right). \tag{8}$$

With the help of this function, we rewrite the rate equation (7) in the equivalent integral form

$$p_n(t) = \int_{-\infty}^{t} dt_L \mathcal{P}_n(t|t_L) \omega(f_{n-1}(t_L)) p_{n-1}(t_L), \tag{9}$$

where we used the initial condition $p_n(-\infty)=0$, meaning that in the infinitely remote past the cantilever was infinitely far away from the nth potential well. While Eq. (9) is suitable for the description of transient processes, we are interested in the long-time limit, when these processes have decayed completely.

Based on the linear character of the experimentally observed time dependence of the lateral force $f(t)$ during the stick part of the motion [3,4], as well as on the simulation results [see Fig. 1(b)], we can make the approximation that as long as the tip is confined to one of the potential wells, the force $f_n(t)$ grows linearly in time. In other words, we neglect the influence of the elastic energy on the position of the minima in Eq. (2) and approximate $z_n(t)$ by $na - vt$ in expression (5) for the elastic force:

$$z_n(t) \simeq na - vt, \quad f_n(t) \simeq \varkappa(vt - na). \tag{10}$$

In view of the time periodicity of the potential (2)—namely, $U(z,t)=U(z,t+a/v)$—the long-time limit of the probabilities of occupying the $(n-1)$st and the nth potential wells, as well as the elastic forces, are related as

$$p_{n-1}(t) = p_n(t + a/v), \quad f_{n-1}(t) = f_n(t + a/v). \tag{11}$$

Furthermore, by making the change of variables according to Eq. (10), we go from the probability $\mathcal{P}_n(t|t_L)$ in the time domain to the probability $\mathcal{P}(f|f_L)$ of staying within the same potential well up to the force value f provided that the initial lower force value at $t=t_L$ was f_L:

$$\mathcal{P}(f|f_L) = \exp\left(- \frac{1}{\varkappa v} \int_{f_L}^{f} df' \, \omega(f') \right). \tag{12}$$

Using Eqs. (11) and (10), we obtain from Eq. (9) the following equation for the probability of realization of a given force value f after the decay of transient processes:

$$p(f) = \frac{1}{\varkappa v} \int_{-\infty}^{f} df' \mathcal{P}(f|f') \omega(f' + \varkappa a) p(f' + \varkappa a), \tag{13}$$

where the now superfluous index n has been omitted, as the force probability distribution is the same in each well.

This integral equation can be used to determine the force probability distribution $p(f)$ iteratively. For stability of the numerical implementation, it is desirable to normalize the distribution to one at each iteration step. However, $p(f)$ is not normalized in the usual sense. Rather, at each moment of time the tip occupies one of the potential wells (2), implying $\Sigma_n p_n(t)=1$, or, going from t to f according to Eq. (10), $\Sigma_n p(f+n\varkappa a)=1$.

To make the numerics more robust, we introduce the long-time probability distribution $W(f_L)$ that a given stick phase of motion begins with the force value in a small interval around f_L [see Fig. 1(b)]. Obviously, this distribution is normalized to 1. Then, $p(f)$ can be expressed in terms of the distribution of initial forces $W(f_L)$ as

$$p(f) = \int_{-\infty}^{f} df_L W(f_L) \mathcal{P}(f|f_L), \tag{14}$$

as the probability to find the force value f for the nth potential well is the probability of survival $\mathcal{P}(f|f_L)$ up to this force averaged over all starting forces f_L. Comparison of Eqs. (14) and (13) leads to the following integral equation for $W(f)$:

$$W(f) = \frac{\omega(f + \varkappa a)}{\varkappa v} \int_{-\infty}^{f+\varkappa a} df_L W(f_L) \mathcal{P}(f + \varkappa a|f_L). \tag{15}$$

Further details on the numerical evaluation of $W(f)$ are given in the Appendix.

Next, we turn to the calculation of the time-averaged force (1) from knowledge of the probability $W(f)$. If the cantilever tip is confined to the nth potential well, the force (10) increases from some starting lower value $f_{L,n}$ to some upper value $f_{U,n}$, where the tip makes a transition to the next well. This transition is accompanied by an instantaneous (on the experimental time-scale) drop of force by the amount [see Eq. (10) and Fig. 1(b)]

$$f_{U,n} - f_{L,n+1} = \varkappa a. \tag{16}$$

Defining the average initial force as $\overline{f_L} = \lim_{N\to\infty}(1/N)\Sigma_{n=1}^{N} f_{L,n} \equiv \int df f W(f)$, we consider the stick-slip motion during the time interval t, when the cantilever tip visits about $\lfloor vt/a \rfloor$ potential wells ($\lfloor \cdots \rfloor$ denotes the integer part). Let $\Delta t_n = (f_{U,n} - f_{L,n})/(\varkappa v)$ be the time spent in the nth well. Then the time-averaged force (1) is

$$\overline{f} = \lim_{t\to\infty} \frac{1}{t} \sum_{n=1}^{\lfloor vt/a \rfloor} \frac{f_{U,n} + f_{L,n}}{2} \Delta t_n = \lim_{t\to\infty} \frac{1}{\varkappa v t} \sum_{n=1}^{\lfloor vt/a \rfloor} \frac{f_{U,n}^2 - f_{L,n}^2}{2}.$$

The limit will not change if we replace $f_{L,n}$ by $f_{L,n+1}$ in the sum. Making this replacement and using Eq. (16), we obtain the following approximation for the time-average elastic force $\overline{f}$ from Eq. (1):

$$\overline{f} = \overline{f_L} + \frac{\varkappa a}{2} \equiv \int_{-\infty}^{\infty} df_L f_L W(f_L) + \frac{\varkappa a}{2}. \tag{17}$$

III. FORCE-VELOCITY RELATION

While the relation (17) between the time-averaged force and the first moment of the distribution $W(f)$ is simple, the iterative determination of the latter distribution according to Eq. (15) is only possible by means of a time-consuming numerical procedure. Therefore, our next goal is to obtain an approximate analytic relation between the average force $\overline{f}$ and velocity v.

To this end, we note that Eq. (15) can be rewritten as

$$W(f) = W(f + \varkappa a) - \frac{\partial}{\partial f}\int_{-\infty}^{f+\varkappa a} df_L \mathcal{P}(f + \varkappa a | f_L) W(f_L), \tag{18}$$

as can be verified by taking the derivative in the last term. Multiplication of both sides of this equation by some function $G(f)$ and integration yield

$$\int_{-\infty}^{\infty} df G(f) W(f) = \int_{-\infty}^{\infty} df G(f - \varkappa a) W(f) + \int_{-\infty}^{\infty} df G'(f - \varkappa a) \int_{-\infty}^{f} df_L \mathcal{P}(f | f_L) W(f_L), \tag{19}$$

where we evaluated the last summand using integration by parts with subsequent change of variables of integration from f to $f+\varkappa a$.

It is possible, in principle, to use this equation as a basis of an alternative numerical scheme for calculation of the probability distribution $W(f)$. Namely, one can start with some concrete functional form $W(f; a_1, a_2, \ldots, a_K)$ of this distribution involving unknown parameters $a_1, a_2, \ldots, a_K$ which describe, e.g., the position of the peak of $W(f)$, the width of this distribution, its asymmetry, etc. In order to find these parameters, one can evaluate both sides of Eq. (19) using the trial ansatz $W(f; a_1, \ldots, a_K)$ and imposing the requirement that this equation be satisfied for $G(f) = f, f^2, \ldots, f^K$. As a result of this procedure, Eq. (19) transforms into K coupled nonlinear equations for the parameters a_k, which are to be found numerically.

The advantage of this approach is that it allows one to deduce an analytic approximation for the distribution $W(f)$. However, as will be demonstrated numerically in Sec. IV, for the accurate determination of the first moment of this distribution, it is sufficient to use the simplest ansatz with one parameter: namely,

$$W(f; \overline{f_L}) = \delta(f - \overline{f_L}), \quad \overline{f_L} \equiv \overline{f} - \varkappa a/2, \tag{20}$$

where we exploited Eq. (17) in the last identity. To motivate this ansatz physically, we first write Eq. (19) with $G(f) = f$:

$$\varkappa a = \int_{-\infty}^{\infty} df_L W(f_L) \int_{f_L}^{\infty} df \mathcal{P}(f | f_L), \tag{21}$$

where we interchanged the order of integration over f and f_L. It can be shown [17] that the inner integral on the right-hand side of this equation represents the average force increment $\Delta F(f_L)$ during a given stick phase, provided that the initial force value was f_L. The expression on the right-hand side, therefore, is the force increment during the stick phase averaged over all initial forces; this quantity equals the force drop $\varkappa a$ during the slip to the next potential well.

Employment of the ansatz (20) is justified if the behavior of the function $\Delta F(f_L) := \int_{f_L}^{\infty} df \mathcal{P}(f | f_L)$ does not deviate strongly from linearity in that force interval around $\overline{f_L}$, where the distribution $W(f_L)$ is significantly different from zero. To see that this condition is indeed reasonably satisfied, let us consider two cases of high and low $\varkappa$.

(i) At high cantilever stiffnesses, the probability of staying within the same well (12) is close to 1 in a rather extended force interval above f_L [because of a large factor $\varkappa$ in the denominator of the expression in the exponent in Eq. (12)]. This means that the statistics of jump events, and hence the average force at the moment of transition, is practically independent of the initial force f_L. Correspondingly, the average force increment for a fixed initial force f_L indeed behaves linearly with f_L—i.e., as $\Delta F(f_L) = \overline{f_U} - f_L$ at high $\varkappa$, where the average upper force $\overline{f_U}$ is practically independent of f_L.

(ii) As a result of a transition from one well to the next, the force experiences an abrupt drop by the amount $\varkappa a$, which, therefore, can be taken as a measure of magnitude of force fluctuations during the stick-slip motion. The width of the distribution $W(f_L)$ is therefore also small at small $\varkappa$, so that the deviations of the function $\Delta F(f_L)$ from linearity can be neglected within the relevant force interval.

Since the ansatz (20) can be applied in the Eq. (21) at low and high $\varkappa$, it can reasonably be expected that the error introduced by this approximation is also not too large for intermediate stiffnesses of the cantilever. With the help of this ansatz, Eq. (21) results in the following implicit force-velocity relation [17]:

$$\int_{\overline{f} - \varkappa a/2}^{\infty} df \exp\left(-\frac{1}{\varkappa v} \int_{\overline{f} - \varkappa a/2}^{f} df' \omega(f') \right) = \varkappa a. \tag{22}$$

For an analytic solution of this equation, we need to further approximate the transition rate so as to be able to evaluate the integral on the left-hand side. We motivate our approximation for $\omega(f)$ as follows. According to the Kramers' theory of thermally activated escape [21] [see also Eq. (32) below], the force-dependent transition rate essentially behaves as $\omega(f) \propto e^{-\Delta U(f)/kT}$, where $\Delta U(f)$ is the force-dependent height of the energy barrier separating the current minimum from the next one. While the rate $\omega(f)$ depends exponentially strongly on force, the energy barrier $\Delta U(f)$ is a much weaker function. Indeed, at low forces it behaves as $\Delta U(f) \approx \Delta U(0) - af/2$, as the distance between two adjacent extrema is $a/2$, while at larger forces we have $\Delta U(f) \propto (\text{const} - f)^{3/2}$ [13]. Such a functional form suggests an expansion of the *logarithm* of frequency about some force value f_0—i.e., to take, to first order,

$$\omega(f) \approx \omega(f_0) e^{\alpha(f_0)(f - f_0)}, \quad \alpha(f) := \omega'(f)/\omega(f). \tag{23}$$

The next question is how to choose the force f_0, about which the expansion is performed. To answer this question, let us examine Eq. (22) more closely. Depending on the value of $\varkappa$, the integrand, $\exp(\cdots)$, may exhibit two kinds of behavior:

(i) At high $\varkappa$, there is a rather wide region of forces between $\overline{f_L}$ and $\overline{f_U}$, where the integrand has the value 1, followed by an abrupt drop to zero in the immediate vicinity of $\overline{f_U}$. The nature of the approximation (23) is such that if we

choose f_0 to lie in the region of the steepest descent of the integrand, we will correctly reproduce its behavior not only in this region, but also outside of it, where the integrand is very close to 0 (at higher forces) or 1 (at lower forces).

(ii) At low $\varkappa$, the integrand drops to zero in a rather narrow interval above $\bar{f}_L = \bar{f} - \varkappa a/2$. Therefore, we expect that the integral will not be very sensitive to the choice of f_0, provided that f_0 belongs to that narrow region where the integrand is notably different from zero. This region extends from $\bar{f}_L$ to a value slightly higher than the average force at the moment of transition, $\bar{f}_U = \bar{f} + \varkappa a/2$ [cf. Eq. (16)].

Thus, the choice of the expansion point in Eq. (23), which applies to both cases equally well, is simply

$$f_0 = \bar{f}_U \equiv \bar{f} + \varkappa a/2. \tag{24}$$

Making a change of variables according to $x = e^{\alpha(\bar{f}_U)(f-\bar{f}_L)}$, we have, from Eqs. (22)–(24),

$$\alpha(\bar{f}_U)\varkappa a = e^{g(\bar{f}_U)} E_1(g(\bar{f}_U)), \quad g(f) := \frac{\omega(f)e^{-\alpha(f)\varkappa a}}{\varkappa v\, \alpha(f)}. \tag{25}$$

Here $E_1(g) = \int_1^\infty dx e^{-gx}/x$ is the exponential integral, which can be evaluated numerically using a standard algorithm [22].

It follows from Eq. (25) that the sought relation between force and velocity has the form

$$v(\bar{f}) = a\omega(\bar{f} + \varkappa a/2) Q\left(\frac{\omega'(\bar{f} + \varkappa a/2)}{\omega(\bar{f} + \varkappa a/2)} \varkappa a \right), \tag{26}$$

where the function $Q(x)$ is defined implicitly by the relation

$$E_1([xe^x Q(x)]^{-1}) e^{[xe^x Q(x)]^{-1}} = x. \tag{27}$$

Equation (26) is the main result of the present work.

From the asymptotic properties of the exponential integral [23] it can be inferred that $Q(x)$ is a monotonically decreasing function with $Q(0)=1$ and $Q(x) \sim e^\gamma/x$ at $x \to \infty$, where $\gamma = 0.577\,215\,664\,9\ldots$ is Euler's constant. We further approximate this function by

$$Q(x) \approx 1/\sqrt{1 + (e^{-\gamma}x)^2}. \tag{28}$$

The high accuracy of this approximation is obvious from Fig. 2.

IV. NUMERICAL RESULTS

It is instructive to test the accuracy of the approximate expression (26) by comparing it with the results obtained numerically from the force probability distribution, Eqs. (15) and (17), for a model system with realistic parameters. To this end, we assume that the surface contribution to the potential (2) can be described by a trigonometric function

$$U_0(z) = -\frac{\Delta U_0}{2} \cos \frac{2\pi z}{a}, \tag{29}$$

with the amplitude $\Delta U_0 = 250$ pN nm and periodicity $a = 0.52$ nm [8]. Furthermore, we assume that the fluctuations

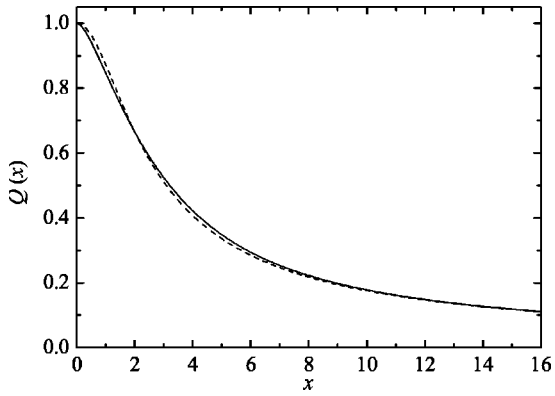

FIG. 2. The function $Q(x)$ appearing in the force-velocity relation (26), as calculated numerically from Eq. (27) (solid line) and the approximation (28) (dashed line).

of the tip coordinate are governed by the overdamped ($m \to 0$) Langevin equation (4) with $kT = 4.04$ pN nm (room temperature), $\eta = 1$ pN msec/nm [13,15], and $\varkappa$ varying between 0.01 and 1 N/m [8,15].

To calculate the force-dependent transition rates $\omega(f)$, we first note that the position of the local potential minimum corresponding to the force value f is given by [cf. Eq. (5)]

$$z_{min} = -f/\varkappa \tag{30}$$

(we use the sign convention, in which $f > 0$ and $z_{min} < 0$). The condition that one of the minima of the potential (2) coincides with $-f/\varkappa$ is met not at arbitrary, but at specific moments of time, t_f, which can be found from the requirement that the derivative of the total potential (2) and (29) at $z = -f/\varkappa$ and $t = t_f$ be zero, i.e., from the equation $U_0'(vt_f - (f/\varkappa)) = f$, leading to

$$t_f = \frac{1}{v}\left[\frac{f}{\varkappa} + \frac{a}{2\pi} \sin^{-1}\left(\frac{af}{\pi \Delta U_0} \right) + na \right]. \tag{31}$$

Here, an integer n marking the minimum can be arbitrary in view of the periodicity of the potential $U_0(z)$. It is a well-known result from Kramers' theory [21] that the transition rate is given by

$$\omega(f) = \omega_0(f) e^{-\Delta U(f)/kT},$$

$$\omega_0(f) = \frac{1}{2\pi\eta} \sqrt{|U''(z_{min}, t_f) U''(z_{max}, t_f)|}, \tag{32}$$

where z_{max} denotes the position of the barrier separating the current minimum z_{min} from the next one and

$$\Delta U(f) = U(z_{max}, t_f) - U(z_{min}, t_f) \tag{33}$$

is its height.

It thus remains to determine the position of the maximum, z_{max}. Although it can be done numerically, such an approach is rather time consuming, because one needs to search for z_{max} at each sampling point of numerical integration of Eq. (15) or (A2). Therefore, an analytic approximation for z_{max} is desirable. Fortunately, the accuracy of the Kramers' rate (32) is most crucially influenced by the accuracy of determination

of the barrier height (33) and to a much lesser degree by the accuracy of determination of its position: since the first derivative of the potential vanishes at its extrema, a first-order error in z_{max} will result in only a second-order error in $\Delta U(f)$ and hence of $\omega(f)$.

To analytically approximate z_{max}, we focus on that half-period of the substrate potential $U_0(z)$ in Eq. (29) to which the extrema z_{min}, z_{max} belong. Within this half-period, the surface potential can be approximated as

$$\widetilde{U}_0(z) = \alpha(z - z_0) - \beta(z - z_0)^3/3, \tag{34}$$

where z_0 ($z_{min} < z_0 < z_{max}$) is the inflection point. The parameters α and β are chosen so as to correctly reproduce the separation $a/2$ between the extrema of $U_0(z)$ and the barrier height ΔU_0. Imposing these two requirements yields

$$\alpha = 3\Delta U_0/a, \quad \beta = 48\Delta U_0/a^3. \tag{35}$$

Including the elastic energy, we obtain an approximation for the total potential (2) in the relevant half-period: namely, $\widetilde{U}(z) = \widetilde{U}_0(z) + \varkappa z^2/2$. It is easily verified by differentiation that the distance between the two extrema of $\widetilde{U}(z)$ is given by

$$z_{max} - z_{min} = 2\sqrt{\frac{\varkappa^2}{4\beta^2} + \frac{\alpha + \varkappa z_0}{\beta}} \approx 2\sqrt{\frac{\varkappa^2}{4\beta^2} + \frac{\alpha - f}{\beta}}, \tag{36}$$

where we further approximated z_0 by $z_{min} = -f/\varkappa$. This replacement does not introduce much of an error provided that $\varkappa(z_0 - z_{min}) \ll \alpha$, which is consistent with the condition (6) of validity of the rate description. Equation (36) gives us the desired approximation for the position of the relevant maximum of the potential $U(z,t)$.

Having determined z_{max}, we calculate the force-dependent barrier height according to Eq. (33). As our additional analysis based on the numerical determination of z_{max} has shown, our approximation has a very good accuracy of Kramers' rate (32) of about 0.1%.

It should be noted that there exists a force value f_* at which the potential barrier vanishes: $\Delta U(f_*) = 0$. This value depends on the concrete model potential; for the one given by Eq. (29) we have $f_* = \pi\Delta U_0/a$ [cf. Eq. (31)]. As stated in the Introduction, the rate description applies when the relevant barrier height is much greater than the thermal energy. This means that the average upper force at the moment of transition to the next minimum must satisfy the inequality

$$\Delta U(\overline{f} + \varkappa a/2) \gg kT. \tag{37}$$

Typically, the barrier height must be greater than the thermal energy at least by about a factor of 5. For the model parameters chosen below Eq. (29), this condition holds for such forces that $\overline{f} + \varkappa a/2 < 0.9 f_* \approx 1.36$ nN. Our numerical calculations were performed only in the force range specified by this inequality.

Presented in Fig. 3 are the numerical results obtained for four values of cantilever spring constant, $\varkappa = 0.01, 0.1, 0.5,$ and 1 N/m. It is obvious from Fig. 3 that our approximate relation (26) (solid lines) is in excellent agreement with the results obtained from numerical solution of Eq. (7) (circles). The discrepancy between the two sets of data is only a fraction of a percent. Additionally, we note a good qualitative agreement with the experimental results reported in [8], although we have not attempted to perform a quantitative fitting. This agreement worsens at relatively high velocities, where the experimental curves of [8] exhibit plateaus. These plateaus, however, appear at forces dangerously close to f_*, where the condition (37) of validity of the rate theory does not hold. Their nature is discussed in the recent work [15].

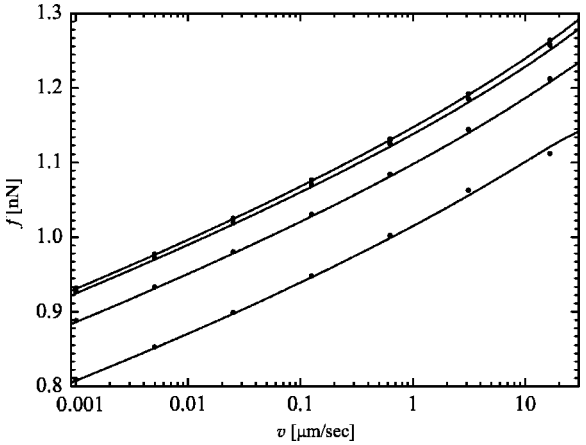

FIG. 3. Time-averaged lateral force vs pulling velocity, as obtained from the relation (26) and the approximation (28) (solid lines) and numerical solution of the integral equation (15) and Eq. (17) (circles). All parameters are the same as in Fig. 1, except for the cantilever spring constants, which are $\varkappa = 0.01$, 0.1, 0.5, and 1 N/m (from top to bottom). Numerical determination of the function $Q(x)$ from Eq. (27) instead of Eq. (28) yields results indistinguishable from the solid lines.

V. RELATION TO THE EXISTING APPROACHES

A description of FFM in terms of occupation probabilities and transition rates has been introduced some time ago [4,8–10,13,14]. The expressions relating pulling velocity and friction force used in Refs. [9,10] and Refs. [4,8,13,14] can be obtained from our relation (26) as limiting cases of small and large cantilever spring constants $\varkappa$, respectively.

When the cantilever has a very low stiffness, we have, from Eq. (26),

$$\lim_{\varkappa \to 0} v(\overline{f}) = a\omega(\overline{f}). \tag{38}$$

This expression has been used earlier, e.g., by Heslot *et al.* [9] and Bouhacina *et al.* [10]. It has a transparent physical meaning. As a result of a transition from one minimum to the next, the force experiences a practically instantaneous (on the experimental time scale) drop by the amount $\varkappa a$, which is a measure of the magnitude of force fluctuations during the stick-slip motion. If it is much smaller than the average force itself—i.e., $\varkappa \ll \overline{f}/a$—then the transitions occur at approximately the same frequency $\omega(\overline{f})$; after each such transition, the cantilever moves by the distance a.

In the limit of large $\varkappa$ [but not large enough to render the combined potential (2) lose its multistable character, so that the condition (6) still holds] we have, from Eqs. (26) and (28),

$$v(\overline{f}) = \frac{\omega^2(\overline{f} + \varkappa a/2)}{\varkappa \omega'(\overline{f} + \varkappa a/2)} e^{\gamma}, \quad \text{large } \varkappa. \tag{39}$$

It can be verified that the force-velocity relations used previously in Refs. [4,8,13,14] have the same structure (note, however, that these works either present the force-velocity relation by expressing the average lateral force as a function of velocity [4,13,14] or as an equation where both force and velocity appear in both sides [8]). In particular, Eq. (39), as well as the analogous relations in [4,8,13,14], predicts an unphysical divergence of velocity in the soft-cantilever ($\varkappa \to 0$) limit. The difference between the expressions given in these works stems from different assumptions about the functional form of $\omega(f)$. By adopting these assumptions, one can reduce our equation (39) to the respective formulas obtained in these works. However, our relation (39) is more general, because, in contrast to these works, it does not rely on any specific functional form of the rate $\omega(f)$.

It is possible within the present approach to find the parameter range in which the high-$\varkappa$ approximation (39) is applicable. It follows from Eqs. (26) and (28) that for this to be the case, the argument of the function $Q(x)$ must be much greater than 1: that is,

$$\frac{\omega'(\overline{f} + \varkappa a/2)}{\omega(\overline{f} + \varkappa a/2)} \varkappa a \gg 1. \tag{40}$$

In the lowest nonvanishing order, the Kramers' rate (32) can be approximated as $\omega(f) \approx \omega(0) e^{af/2kT}$, as the distance between the minimum and maximum is about $a/2$. The condition of validity of the high-$\varkappa$ limit (39) is thus seen to be

$$\varkappa a^2/2 \gg kT. \tag{41}$$

Keeping in mind that at room temperature $kT \approx 4$ pN nm and $a \approx 0.5$ nm, we conclude that Eq. (39) is a good approximation for $\varkappa \gg 0.03$ N/m. The large-$\varkappa$ expression (39) in various forms has been used for analysis of experimental data in [4,8]. Yet its applicability limits have not been discussed so far in the literature, and therefore the result (41) is of immediate relevance to experimental nanofriction.

A further difference between our expression (39) and the respective formulas in [4,8,13,14], which is of still greater importance for the analysis of experimental data, is that the factor e^{γ} is absent in these works. By analyzing the problem of escape from a metastable potential well under the action of a steadily increasing force, it can be shown [24,25] that this difference stems from the fact that we use the *average* force at the transition, $\overline{f_U} = \overline{f} + \varkappa a/2$, as an argument, while the authors of [4,8,13,14] work with *the most probable* force f_m found from the maximization of the transition probability $-(\partial/\partial f)\mathcal{P}(f|\overline{f_L})$. In Refs. [4,8], the implicit assumption is made that the most probable force at the transition, f_m, is practically the same as the average force $\overline{f_U}$, which is determined experimentally. To evaluate the effect of this assumption on fitting the experimental results in [4,8], we note the following. The attempt frequency ω_0 in Kramers' rate (32) is assumed to be a force-independent constant in these works. With this additional assumption it is obvious that in order to recover the fitting formulas used in [4,8] from Eq. (39), one only needs to absorb the factor e^{γ} into ω_0. Therefore, the attempt frequency ω_0 is overestimated in Refs. [4,8] by a large factor $e^{\gamma} \approx 1.78$.

VI. CONCLUSIONS

Based on escape rate theory, we have deduced an approximate relation (26) between pulling velocity and the resulting time-averaged friction force acting during the stick-slip motion of an AFM cantilever. The high accuracy of this relation was verified by comparison with the results obtained from the numerically calculated force probability distribution. The analogous relations existing in the literature were shown to be the low- and high-stiffness limits of our result.

One of the most drastic simplifications made in this work is that the motion of the cantilever is essentially one-dimensional, whereas in reality the cantilever tip also moves in the direction perpendicular to that of pulling. An extension of the Tomlinson model to the more general two-dimensional case is treated numerically in [18–20]. The qualitative difference from the one-dimensional case studied here is that the cantilever tip has several choices of the next minima to jump into from the current minimum of the potential. It follows from Langer's generalization of Kramers' theory to many dimensions [21] that the tip will follow the path of the "least resistance" with the highest probability; i.e., it will jump to that minimum which is separated by the smallest barrier. Thus, the motion of the tip will no longer proceed along a straight line, but rather follow a zigzag path. Although this is still a one-dimensional manifold, the rate of transitions from one node to the next will vary, whereas it is the same in the one-dimensional case considered here. However, the model treated in the present work still applies to the two-dimensional case when pulling proceeds along such a crystallographic direction that the internode transition rates remain the same along the path; e.g., for a square underlying lattice, these are the $\langle 01 \rangle$ and $\langle 11 \rangle$ directions. In this sense, the one-dimensional model studied in this work is a special case of the more general two-dimensional model, whose development is an interesting subject for future research.

ACKNOWLEDGMENTS

We are grateful to the Alexander von Humboldt Foundation, the Deutsche Forschungsgemeinschaft (Grant Nos. SFB 613 and RE 1344/3-1), and the ESF-program STOCHDYN for financial support of this work.

APPENDIX

Relation (15) is not very efficient for numerical implementation, because the integral kernel on the right-hand side depends on two arguments f and f_L. This means that for N

sampling points, N^2 evaluations of the kernel are necessary. To cure this difficulty, we present the distribution function of the starting forces in the form

$$W(f) = \omega(f + \varkappa a)\mathcal{P}(f + \varkappa a|-\infty)g(f), \tag{A1}$$

with the unknown function $g(f)$ satisfying the following integral equation, in which the kernel depends on only one argument f_L:

$$g(f) = \frac{1}{\varkappa v}\int_{-\infty}^{f+\varkappa a} df_L \omega(f_L + \varkappa a)\mathcal{P}(f_L + \varkappa a|f_L)g(f_L). \tag{A2}$$

It was this equation that we solved iteratively with the integral evaluated numerically at each iteration step.

[1] G. Binnig, C. F. Quate, and Ch. Gerber, Phys. Rev. Lett. **56**, 930 (1986).
[2] C. M. Mate, G. M. McClelland, R. Erlandsson, and S. Chiang, Phys. Rev. Lett. **59**, 1942 (1987).
[3] A. Socoliuc, R. Bennewitz, E. Gnecco, and E. Meyer, Phys. Rev. Lett. **92**, 134301 (2004).
[4] E. Gnecco, R. Bennewitz, T. Gyalog, Ch. Loppacher, M. Bammerlin, E. Meyer, and H.-J. Güntherodt, Phys. Rev. Lett. **84**, 1172 (2000).
[5] S. Sills and R. M. Overney, Phys. Rev. Lett. **91**, 095501 (2003).
[6] R. Bennewitz, T. Gyalog, M. Guggisberg, M. Bammerlin, E. Meyer, and H.-J. Güntherodt, Phys. Rev. B **60**, R11301 (1999).
[7] E. Gnecco, R. Bennewitz, T. Gyalog, and E. Meyer, J. Phys.: Condens. Matter **13**, R619 (2001).
[8] E. Riedo, E. Gnecco, R. Bennewitz, E. Meyer, and H. Brune, Phys. Rev. Lett. **91**, 084502 (2003).
[9] F. Heslot, T. Baumberger, B. Perrin, B. Caroli, and C. Caroli, Phys. Rev. E **49**, 4973 (1994).
[10] T. Bouhacina, J. P. Aimé, S. Gauthier, D. Michel, and V. Heroguez, Phys. Rev. B **56**, 7694 (1997).
[11] M. A. Lantz, S. J. O'Shea, M. E. Welland, and K. L. Johnson, Phys. Rev. B **55**, 10776 (1997).
[12] K. L. Johnson and J. Woodhouse, Tribol. Lett. **5**, 155 (1998).
[13] Y. Sang, M. Dubé, and M. Grant, Phys. Rev. Lett. **87**, 174301 (2001).
[14] O. K. Dudko, A. E. Filippov, J. Klafter, and M. Urbakh, Chem. Phys. Lett. **352**, 499 (2002).
[15] P. Reimann and M. Evstigneev, Phys. Rev. Lett. **93**, 230802 (2004); New J. Phys. **7**, 25 (2005).
[16] T. Baumberger and C. Caroli, Eur. Phys. J. B **4**, 13 (1998).
[17] M. Evstigneev and P. Reimann, Europhys. Lett. **67**, 907 (2004).
[18] T. Gyalog, M. Bammerlin, R. Lüthi, E. Meyer, and H. Thomas, Europhys. Lett. **31**, 269 (1995).
[19] H. Hölscher, U. D. Schwarz, and R. Wisendanger, Europhys. Lett. **36**, 19 (1996).
[20] C. Fusco and A. Fasolino, Phys. Rev. B **71**, 045413 (2005).
[21] P. Hänggi, P. Talkner, and M. Borkovec, Rev. Mod. Phys. **62**, 251 (1990).
[22] W. H. Press, S. A. Teukolsky, W. T. Vetterling, and B. P. Flannery, *Numerical Recipies in C* (Cambridge University Press, Cambridge, England, 1999).
[23] *Handbook of Mathematical Functions*, edited by M. Abramowitz and I. Stegun (Dover, New York, 1965).
[24] P. W. Williams, Anal. Chim. Acta **479**, 107 (2003).
[25] A. Garg, Phys. Rev. B **51**, 15592 (1995).